Proton Inelastic Scattering on ^{56}Ni in Inverse Kinematics

G. Kraus, P. Egelhof, C. Fischer, H. Geissel, A. Himmler, F. Nickel, G. Münzenberg, W. Schwab, and A. Weiss
Gesellschaft für Schwerionenforschung, D-64220 Darmstadt, Germany

J. Friese, A. Gillitzer, H. J. Körner, and M. Peter
Technische Universität München, D-85748 Garching, Germany

W. F. Henning and J. P. Schiffer
Argonne National Laboratory, Argonne, Illinois 60439

J. V. Kratz
University of Mainz, D-55099 Mainz, Germany

L. Chulkov, M. Golovkov, and A. Ogloblin
I. V. Kurchatov Institute, Moscow, Russia

B. A. Brown
Michigan State University, East Lansing, Michigan 48824
(Received 19 May 1994)

Inelastic proton scattering to the first excited 2^+ state of the doubly magic ^{56}Ni nucleus was investigated in inverse kinematics, using a secondary beam of radioactive ^{56}Ni nuclei. At an incident energy of 101 MeV/nucleon, a value $B(E2, 0^+ \rightarrow 2^+) = 600 \pm 120\ e^2\,\mathrm{fm}^4$ was measured. This result completes the set of experimental data for the first excited 2^+ states in the $1f$-$2p$ shell with a closed shell of neutrons or protons. These data are compared to recent shell-model calculations.

PACS numbers: 25.40.Ep, 23.20.Js, 25.60.+v, 27.40.+z

The availability of radioactive beams of good quality opens a new regime for nuclear structure studies through the use of direct reactions in inverse kinematics. In particular, nuclei become accessible to experiments in the region of shell closures away from stability (for example ^{56}Ni, ^{132}Sn), nuclei that are often important in astrophysical scenarios for element synthesis. ^{56}Ni is a doubly closed-shell nucleus, well known for its major role in stellar nucleosynthesis: For instance the decay in the light curve of supernova 1987A was dominated over the first year by the mass 56 decay curve, and the solar systems abundance of ^{56}Fe is a result of the stability of ^{56}Ni. Nucleon stripping and pickup reactions and inelastic scattering can provide valuable information on the single-particle states that are the foundation of our understanding of nuclear structure, on the matrix elements of the effective nucleon-nucleon interaction, on collective excitations, and on neutron-capture cross sections of astrophysical interest in regions that so far have been inaccessible.

As a first such experiment with a medium-heavy nucleus, elastic and inelastic proton scattering on ^{56}Ni have been investigated in inverse kinematics at $E_{\mathrm{lab}} =$ 101 MeV/nucleon. The experiment, performed at the SIS accelerator at GSI, Darmstadt, was intended to provide a more accurate value of the poorly known matrix element [1] for the transition connecting the 0^+ ground state to the first excited 2^+ state at 2.7 MeV in ^{56}Ni. A successful measurement would complete the data set of first excited 2^+ excitations for N and/or $Z = 28$ nuclei in the $1f$-$2p$ shell and provide a sensitive test of recent shell-model calculations.

The measurement focused on the inelastic cross section in the vicinity of the first diffraction maximum in the angular distribution. It occurs in the favorable region of the kinematics of the inverse reaction where the largest center-of-mass angular range is covered in a limited range of laboratory angles, an interval of about 2° around $\theta_{\mathrm{lab}} = 79.1°$ [Fig. 1(a)]. Because of the kinematics and the large level spacing in ^{56}Ni, the measurement can provide unambiguous excitation spectra, even with a spread in beam energy of several percent. This favorable situation allowed us to perform this experiment with a relatively low-quality secondary beam ($\Delta E_{\mathrm{lab}} \approx 2\%$, $\varepsilon \approx 20\pi$ mm mrad), limited by the fragmentation process.

The ^{56}Ni beam was obtained via fragmentation of a primary beam of ^{58}Ni, 2×10^8/s at 350 MeV/nucleon, incident on a 4 g/cm^2 beryllium target. The isotopes among the fragmentation products were separated in flight by the GSI Fragment Separator (FRS) [2]. The FRS is a large ($\approx$ 70 m length) zero-degree magnetic spectrometer operated in the achromatic mode. It combines magnetic rigidity and energy-loss separation; for the latter a profiled aluminum degrader was used with a total thickness of about half the range of the fragments. It provides full

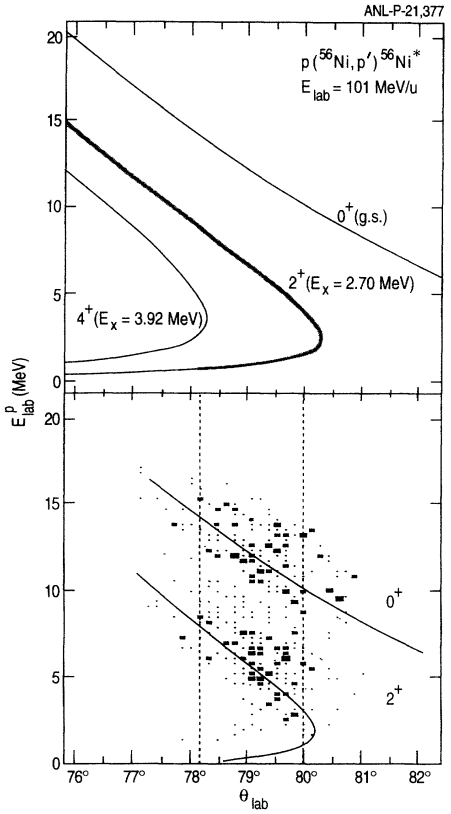

FIG. 1. Top: Kinematics of proton energy $E_{\rm lab}^{p}$ vs proton scattering angle $\theta_{\rm lab}$ for the inverse reaction $p(^{56}\mathrm{Ni}, p')^{56}\mathrm{Ni}^*$. The narrow shadowed area around the curve for the first excited 2^+ state (E_x = 2.70 MeV) indicates the spread expected from a ±1% width in the incident beam energy. Bottom: Scatter plot of measured energy $E_{\rm lab}$ vs scattering angle $\theta_{\rm lab}$ for the recoil protons. The solid curves are again the kinematics, but corrected for energy losses in the target. The dotted lines indicate the (purely geometrical) acceptance limits in the scattering angle from the known detector geometry.

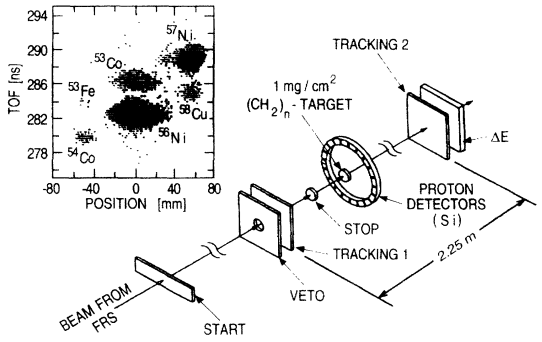

FIG. 2. Experimental setup for ^{56}Ni beam tracking and recoil-proton detection. The inset shows the isotope separation obtained with the GSI Fragment Separator FRS via time-of-flight (TOF) and focal-plane position measurement.

isotopic and element selectivity and, in our case, up to 10^5/s secondary ^{56}Ni ions of 101 MeV/nucleon energy.

The experimental setup consisted of two detector systems: One to identify the fragments behind the FRS and to enable their individual tracking, and a second to detect the recoil protons from the scattering experiment. This configuration is shown schematically in Fig. 2. The fragment identification system consists of a set of thin plastic scintillation detectors (0.5–2 mm thickness). The flight time was measured between the midplane and the final plane of the fragment separator over a distance of ≈36 m, with a time resolution of about 200 ps. Together with an energy-loss measurement in a 2-mm-thick plastic scintillation counter and the focal-plane position measurement with two position-sensitive 0.5-mm-thick plastic scintillators, the mass A, the nuclear charge Z, and the trajectory angle of the transmitted fragments are identified unambiguously (see inset in Fig. 2). A position resolution of $\Delta x \leq 1$ mm was observed, and the operation of the scintillators allowed for beam intensities up to 10^5 s^{-1}.

The ^{56}Ni beam with an average intensity of 2×10^4/s, a divergence of 7 mrad (FWHM), and a beam spot with a diameter of 15 mm (FWHM) was incident on a 1 mg/cm^2 $(CH_2)_n$ target. The recoil protons were detected at a distance of 20 cm from the target in a ring of 19 silicon detectors, 2500 μm thick and 50×10 mm^2 active area each, extending over the complete azimuthal circle and positioned at the laboratory angle of $\theta_{\rm lab} = 79.1°$, corresponding to the region of the diffraction peak in the inelastic scattering. Particle identification of the recoiling protons was done by time of flight. The background originating from ^{56}Ni + ^{12}C collisions was measured with pure carbon targets and subtracted from the $(CH_2)_n$ yield. The two-dimensional position-sensitive detectors permitted the determination of the direction and the incident angle of individual beam particles in the poor-emittance secondary beam. From these measurements and from the proton energy measured in the silicon detectors, the energy vs scattering angle distribution shown in Fig. 1 was constructed. Elastic scattering and inelastic scattering to the first excited state of ^{56}Ni are clearly identified and well separated.

On the left side of Fig. 3 the measured proton energy spectrum for the $p(^{56}\mathrm{Ni}, p')^{56}\mathrm{Ni}^*$ reaction is shown together with a Monte Carlo simulation, which takes into account the full geometry and the response of the experimental setup, the beam emittance, as well as the energy loss and multiple scattering of the recoil protons in the target. The theoretical angular distributions used in the simulations are calculated with the coupled-channels code CHUCK [3] with optical-model parameters derived from 100 MeV proton scattering on ^{58}Ni [4]. Very good agreement is observed between the shapes of the predicted and measured spectra. The relevant center-of-mass angular interval for elastic scattering corresponds to a region where the angular distribution shows a minimum near 22°, which

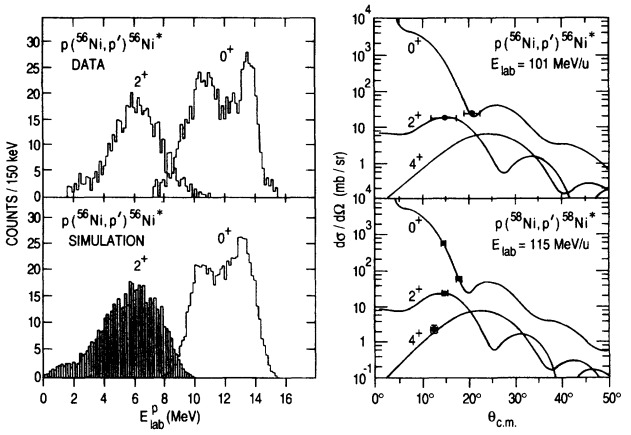

FIG. 3. Experimental (left top) and simulated (left bottom) yields for the recoil protons from the reaction $p(^{56}\mathrm{Ni}, p')^{56}\mathrm{Ni}^*$ as a function of proton energy E^p_{lab} (see Fig. 1). On the right side, data points and coupled-channel Born-approximation predictions are plotted for the angular distributions of elastic and inelastic proton scattering for a (radioactive) ^{56}Ni (top) and a (stable) ^{58}Ni beam (bottom).

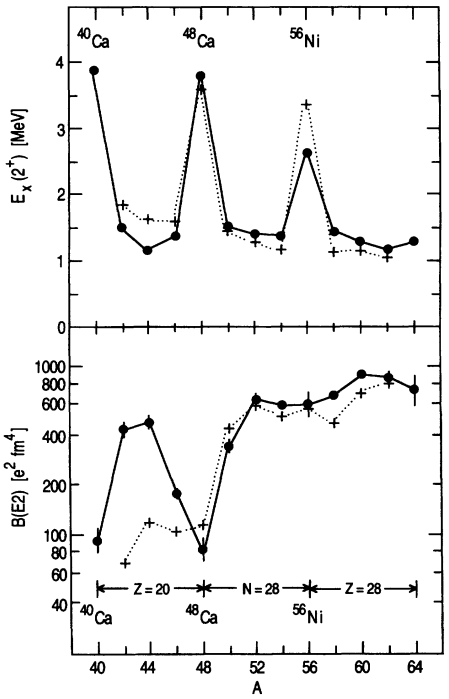

FIG. 4. Experimental excitation energies (top) and $B(E2)$ values (bottom) for excitation to the first excited 2^+ states in N and/or $Z = 20$ or 28 nuclei of the $1f$-$2p$ shell. The solid lines are to guide the eye. The dotted curves represent the shell-model predictions discussed in the text. The experimental values for the $B(E2)$ are from Ref. [1].

is reflected in a minimum in the energy spectrum of the protons near 12 MeV. Both of these effects are seen in Fig. 3.

The absolute normalization was obtained from the known target thickness and by directly counting the incident ^{56}Ni "beam" particles on the first position-sensitive detector. As a test of the technique, the same measurement was also carried out with a (stable) ^{58}Ni beam. The measured elastic cross sections for ^{58}Ni coincide within 1% with predicted values from an optical model calculation with parameters from an earlier experiment at 100 MeV proton energy [4] (this good agreement is of course fortuitous in view of the systematic uncertainty which we estimate to be around 5%).

To extract a matrix element from the inelastic excitation, the coupled-channels calculation with a form factor that was the derivative of the optical potential was used. For the ^{56}Ni 2^+ excitation, a value of $\beta = 0.173 \pm 0.017$ was obtained which then corresponds to a value of $B(E2) = 600 \pm 120\ e^2\,\mathrm{fm}^4$. The uncertainties include our estimate of systematic errors. The only previous value for ^{56}Ni, a lower limit of $B(E2) \geq 230\ e^2\,\mathrm{fm}^4$, quoted in the Nuclear Data Sheets [1], is based on a lifetime measurement yielding 76^{+49}_{-24} fs for the 2^+ state [5]. We also note that the analysis of the present data for the 2^+ state ^{58}Ni yields a value of $\beta = 0.22 \pm 0.02$, which is reasonably consistent with the "adopted" value from the compilation in Ref. [1], $\beta = 0.18 \pm 0.01$.

The present result for a radioactive nucleus completes the systematics of experimental $B(E2)$ values for the first excited 2^+ states of nuclei with N and/or $Z = 20$ or 28. The $B(E2)$ values of these nuclei are plotted in Fig. 4, together with the excitation energies of the first 2^+ states. For the doubly magic nuclei ^{40}Ca, ^{48}Ca, and ^{56}Ni, the excitation energies exceed those of neighboring (N and/or $Z = 20$ or 28) nuclei by a factor of 2 to 3. The inverse behavior is observed for the $B(E2)$'s, except for ^{56}Ni. In the simplest picture, all three nuclei have good shell closure in the ground state, lowering the ground-state energy and raising the energy of the first excited state. Correspondingly, the $B(E2)$'s are low in ^{40,48}Ca and then increase with proton occupation as the proton $f_{7/2}$ shell is filled. In ^{56}Ni the proton $f_{7/2}$ shell should be inert, and one might have expected a low value of $B(E2)$ as in ^{40}Ca. Instead, the proximity of the $f_{5/2}$-$p_{3/2}$-$p_{1/2}$ orbits seems to compensate for the doubly magic core, and the $B(E2)$ value is the same, within uncertainties, as for the neighboring $^{52}_{24}\mathrm{Cr}_{28}$, $^{54}_{26}\mathrm{Fe}_{28}$, and $^{58}_{28}\mathrm{Ni}_{30}$.

More quantitatively, Fig. 4 shows shell-model predictions based on an effective interaction obtained recently for the lower part of the $1f$-$2p$ shell [6]. One sees good agreement with the trends in the data, except for the non-closed-shell Ca nuclei, where core excitations play a role. For the Ca isotopes the full $1f$-$2p$ model space and neutron effective charge of $e_n = 0.64e$ were used. For the $N = 28$ isotones the $1f$-$2p$ shell-model space was truncated to include only

the $(1f_{7/2})^{A-40-r}(1f_{5/2}, 2p_{3/2}, 2p_{1/2})^r$ configurations, and for the Ni isotopes the truncation was to $(1f_{7/2})^{16-r}(1f_{5/2}, 2p_{3/2}, 2p_{1/2})^{A-56+r}$ configurations, where in both cases $r = 0$ or 1. Within the truncated model space, effective charges (obtained by an overall adjustment to data) of $e_p = 1.4e$ and $e_n = 0.9e$ were used. This truncation is justified by the relatively high excitation energies in ^{48}Ca and ^{56}Ni. Also, for the $N = 28$ calculations, the single-particle energies were readjusted to fit the data from the odd-A nuclei around ^{48}Ca and ^{56}Ni [e.g., Figs. 3-2(d) and 3-2(e) in Ref. [7]] and then interpolated in between. Correct single-particle energies are the minimal and primary concern of any effective shell-model Hamiltonian.

The $B(E2)$ were calculated with harmonic-oscillator radial wave functions with $\hbar\omega = 45A^{-1/3} - 25A^{-2/3}$ [MeV]. The effective charges of $e_p = 1.4e$ and $e_n = 0.9e$ are somewhat larger than the typical values needed in the full $1f$-$2p$ space [6] ($e_p = 1.33e$ and $e_n = 0.64e$) because of the truncation made within the $1f$-$2p$ shell. Effective charges are needed in the full $1f$-$2p$ model space to take into account coupling with the giant quadrupole resonance [8]. In ^{56}Ni the first excited 2^+ state is an isoscalar one-particle–one-hole configuration with a relatively large $B(E2)$ because of the large coherent $1f_{7/2} \rightarrow 2p_{3/2}$ and $1f_{7/2} \rightarrow 1f_{5/2}$ contributions. The structure is similar for ^{48}Ca, but there only neutrons are excited and the $B(E2)$ is smaller. The first excited 2^+ states for the other $N = 28$ isotones have primarily $(1f_{7/2})^{A-40}$ configurations which are lower in energy and have intrinsically weaker $B(E2)$ values, but these then couple coherently to the 1p-1h excitations resulting in a slightly lower energy and a much larger $B(E2)$. A similar result is obtained for the $^{58\text{-}64}$Ni isotopes with $(1f_{5/2}, 1p_{3/2}, 1p_{1/2})^{A-56}$ configurations coupled coherently to the 1p-1h excitation. It is interesting to note that a remnant of the 1p-1h excitation exists at 3–4 MeV excitation in the non-closed-shell $N = 28$ and Ni isotopes, with about one-third of the non-energy-weighted $E2$ strength and about one-half of the energy-weighted $E2$ strength (i.e., the part within the $1f$-$2p$ model space and not including the giant quadrupole strength).

Recent advances in shell-model calculations based on path integrals and the introduction of novel Monte Carlo techniques allow treatment of the full $1f$-$2p$ shell with realistic interactions and all modes of excitation [9]. This is a very promising approach. However, for technical reasons, until now only total $B(E2)$ strengths from the ground state to all 2^+ states are predicted for the fp shell nuclei under study here, and thus the results of these calculations do not readily lend themselves to a direct comparison with the present data without further assumptions.

We thank the GSI accelerator staff for their untiring efforts to produce good intensity secondary ^{56}Ni beams and S. Koonin and K. Langanke for communicating the results of their shell-model calculations with Monte Carlo techniques prior to publication. B. A. B. acknowledges support from the Alexander von Humboldt Foundation and from NSF Grant No. 94-03666. This research was partially supported by the U. S. Department of Energy under Contract No. W-31-109-Eng-38.

[1] S. Raman, C. H. Malarkey, W. T. Milner, C. W. Nestor, Jr., and P. H. Stelson, At. Data Nucl. Data Tables **36**, 1 (1987).

[2] H. Geissel, P. Armbruster, K. H. Behr, A. Brünle, K. Burkard, M. Chen, H. Folger, B. Franczak, H. Keller, O. Klepper, B. Langenbeck, F. Nickel, E. Pfeng, M. Pfützner, E. Roeckl, K. Rykaczewski, I. Schall, D. Schardt, C. Scheidenberger, K.-H. Schmidt, A. Schröter, T. Schwab, K. Sümmerer, M. Weber, G. Münzenberg, T. Brohm, H.-G. Clerc, M. Fauerbach, J.-J. Gaim, A. Grewe, E. Hanelt, B. Knödler, M. Steiner, B. Voss, J. Weckenmann, C. Ziegler, A. Magel, H. Wollnik, J. P. Dufour, Y. Fujita, D. J. Vieira, and B. Sherrill, Nucl. Instrum. Methods Phys. Res., Sect. B **70**, 286 (1992).

[3] P. D. Kunz *et al.*, CHUCK—A Coupled-Channel Code, The Niels Bohr Institute Computer Program Library, 1977.

[4] K. Kwiatkowski and N. S. Wall, Nucl. Phys. **A301**, 349 (1978).

[5] N. Schulz, J. Chevallier, B. Haas, J. Richert, and M. Toulemonde, Phys. Rev. C **8**, 1779 (1973).

[6] W. A. Richter, M. G. van der Merwe, R. E. Julies, and B. A. Brown, Nucl. Phys. **A523**, 325 (1991).

[7] A. Bohr and B. R. Mottelson, *Nuclear Structure* (W. A. Benjamin, New York, 1969), Vol. 1.

[8] H. Sagawa and B. A. Brown, Nucl. Phys. **A430**, 84 (1984).

[9] G. H. Lang, C. W. Johnson, S. E. Koonin, and W. E. Ormand, Phys. Rev. C **48**, 1518 (1993); D. J. Dean, P. B. Radha, K. Langanke, Y. Alhassid, S. E. Koonin, and W. E. Ormand, Phys. Rev. Lett. **72**, 4066 (1994).

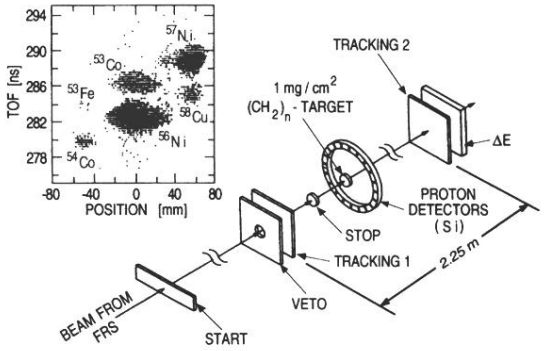

FIG. 2. Experimental setup for ^{56}Ni beam tracking and recoil-proton detection. The inset shows the isotope separation obtained with the GSI Fragment Separator FRS via time-of-flight (TOF) and focal-plane position measurement.

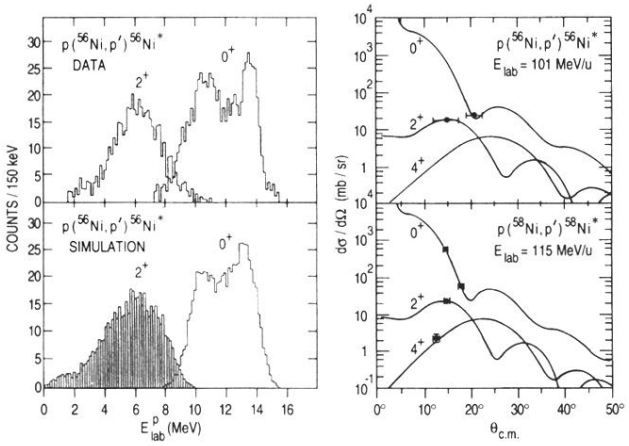

FIG. 3. Experimental (left top) and simulated (left bottom) yields for the recoil protons from the reaction $p(^{56}\mathrm{Ni}, p')^{56}\mathrm{Ni}^*$ as a function of proton energy E^p_{lab} (see Fig. 1). On the right side, data points and coupled-channel Born-approximation predictions are plotted for the angular distributions of elastic and inelastic proton scattering for a (radioactive) ^{56}Ni (top) and a (stable) ^{58}Ni beam (bottom).